

Acoustic, opto-acoustic, and thermal properties investigated around the phase transitions of NaCN and $\text{Na}(\text{CN})_x\text{Cl}_{1-x}$ mixed crystals

J. K. Krüger, R. Jiménez, K.-P. Bohn, J. Petersson, J. Albers, A. Klöpperpieper, E. Sauerland, and H. E. Müser
Fachbereich Physik, Universität des Saarlandes, Gebäude 38, D-6600 Saarbrücken, Federal Republic of Germany

(Received 9 February 1990)

The elastic and opto-acoustic properties of sodium cyanide crystals NaCN and sodium cyanide-sodium chloride mixed crystals $\text{Na}(\text{CN})_x\text{Cl}_{1-x}$ ($1 \geq x \geq 0.63$) were investigated below room temperature using high-resolution Brillouin spectroscopy. Employing special scattering techniques, we were able to measure the elastic behavior in both the high- and low-temperature phases. Changing from systems with high CN^- concentrations, which undergo structural phase transitions of first order, to systems with low CN^- concentrations, which show glass transitions, the discontinuities of the extremely soft shear stiffness of these cubic crystals gradually vanish. Using a space- and angular-resolving Brillouin technique, we report data on the inhomogeneity of the Czochralski-grown mixed crystals. The consequences of these inhomogeneities for the phase-transition behavior have been studied by thermal analyses. We try to describe our shear elastic stiffness data in the framework of current theoretical approaches.

I. INTRODUCTION

Molecular crystals of type $M(\text{CN})_xY_{1-x}$, where M^+ is an alkali metal and Y^- is a halogen ion, show an orientational disorder of the CN^- ions in the cubic high-temperature phase. At concentrations x above a so-called critical concentration x_c these materials undergo ferroelastic phase transitions with the pure shear mode being the soft mode.^{1-4(a)} Accordingly, the elastic shear stiffness modulus c_{44} (Voigt notation) decreases strongly on approaching the first-order transition temperature. Depending on the composition and the concentration further low-temperature phases may occur in these materials. For concentrations below x_c the materials conserve their cubic structure until the lowest temperatures. The shear stiffness c_{44} of these materials ($x < x_c$) varies completely continuously as a function of temperature T but shows a minimum that indicates a memory of the acoustic soft mode existing at higher concentrations.^{3,5-8} With decreasing concentration the $c_{44}(T)$ curve is shifted upwards in the way that the position of the minimum shifts to lower temperatures, and its depth decreases. Generally, below the minimum of the $c_{44}(T)$ curve an acoustic loss maximum is observed. It is widely believed that both the minimum and the maximum are shifted to lower temperatures with decreasing test frequency. The minimum has been explained by assuming a coupling between rotational and translational degrees of freedom and quenched strain fields. Different theoretical attempts have been made to explain the static elastic properties in the framework of this approach (e.g., Refs. 18 and 19). The acoustic loss maximum is frequency dependent.^{4(b)-6} This dynamical behavior of the acoustic properties is taken as a hint for the appearance of a dynamical glass transition^{4(b),5} in the sense of the α process discussed for the glass transition in polymers.^{9,10}

Most studies of the elastic properties of $M(\text{CN})_xY_{1-x}$

mixed crystals have been devoted to the problem of the orientational glassy state and the corresponding glass transition. Great attention was paid to the temperature and concentration dependence of the elastic stiffness coefficient c_{44} in order to understand the influence of the halogen impurities on the glass transition and the ferroelastic phase transition. Information about the elastic properties of the ferroelastically ordered phases is, according to our knowledge, not available (see, e.g., Refs. 1-3 and 6). This is due to the fact that Brillouin as well as ultrasonic measurements are very much complicated by the formation of differently oriented domains below the transition temperature T_c .

In this work we present a space- and angular-resolving Brillouin technique that enabled us to overcome at least partially the problem of sample opacity caused below T_c by the multidomain structure. These Brillouin techniques have been applied to pure NaCN as well as to $\text{Na}(\text{CN})_x\text{Cl}_{1-x}$ mixed crystals to get information on their elastic properties around their phase transitions. To get an idea about the elastic behavior at the crossover from the first-order phase transition to the continuous glass transition an effort was made to investigate the elastic behavior extremely close to the critical concentration $x_c \approx 0.63$.

Large $\text{Na}(\text{CN})_x\text{Cl}_{1-x}$ mixed crystals and also pure NaCN crystals are generally grown from the melt using the Czochralski technique. Crystals with serious concentration inhomogeneities may result from this growth technique. It is well known¹¹⁻¹³ that due to the monotonous increase of the liquidus and solidus curves from the melting point of NaCN to that of NaCl the ratio of CN^- to Cl^- within the crystal increases monotonically from the seed region to the opposite end. A systematic investigation of the concentration distribution and its influence on the physical properties of these materials has not been performed yet. We present such studies based on investi-

gations of the thermal behavior and of the elastic behavior as determined by space-resolving Brillouin measurements. Special attention has also been paid to the confusing influence of mosaic structures on the elastic properties already existing in the cubic phase. In this context discrepancies appearing between ultrasonic and hypersonic data of NaCN (Refs. 14–16) are discussed. In order to estimate the influence of hypersonic dynamics we discuss the properties of the opto-acoustic dispersion function introduced previously.^{17,27}

Our experimental results will be interpreted using the theoretical model of Michel^{18,19} yielding model parameters that should be the same for the pure and the mixed systems. The agreement with the theory is fairly good but can be further improved introducing a linear temperature-dependent term.

II. EXPERIMENTAL

Crystals were grown from the melt in a Leybold-Heraeus EKZ 250 crystal growth system using an inductively heated Pt crucible under argon atmosphere, which was exchanged several times before reaching the melting temperature. The growth procedure was started with seeds, beginning at the CN⁻ side (with the large lattice constant) increasing the melt ansatz of Cl⁻ in steps of about 10 mol%. The new seed was always prepared from the previously grown crystal.

The CN⁻ content of the grown material could be determined by measuring C and N by an automatic C-H-N analyzer. This method was used to establish the

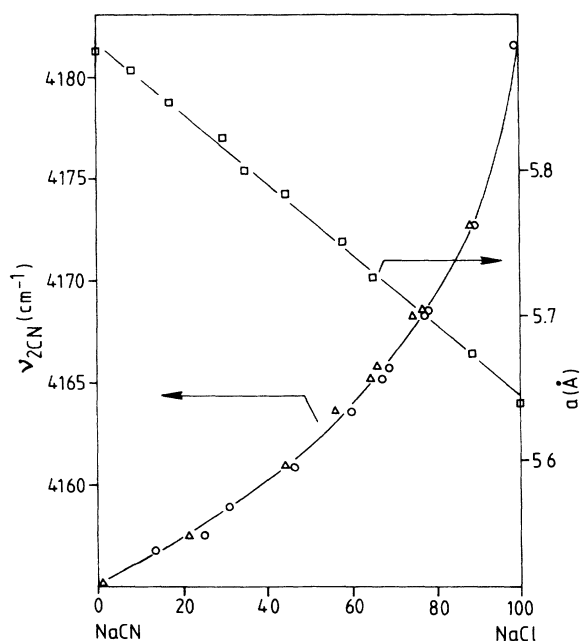


FIG. 1. Dependencies of the lattice constant measured on powdered samples (right scale) and of the frequency of the second harmonic of the CN⁻ stretching vibration (left scale) on the Cl⁻ concentration given in mol.% in mixed single crystals Na(CN)_xCl_{1-x}. Triangles and circles indicate Cl⁻ concentrations obtained from C and N concentrations, respectively, determined by the chemical bond method.

dependence of the lattice constant on the CN⁻ concentration as shown in Fig. 1. The lattice constants were determined with an x-ray goniometer on powdered samples. The rather broad lines [full width at half maximum about 0.3° with Cu K α at the (200) reflex in the mixed crystals] limit the absolute accuracy of the CN⁻ determination from x-ray measurements to about 2%. The main difference between the data in Fig. 1 and earlier published ones²⁰ results from the lattice constant of NaCN reported there for room temperature (5.83 Å).

For the nondestructive CN⁻ determination of cleaved or polished samples, advantage was taken of the dependence of ir-absorption lines on the CN⁻ concentration. Figure 1 shows the dependence of the second harmonic frequency of the CN⁻ stretching vibration on the Cl⁻ concentration as determined with a Nicolet MX-5 Fourier transform infrared spectrometer. Using the curve in Fig. 1, from ir measurements the CN⁻ content could be determined. In order to achieve a sufficient intensity, rather large samples of increasing thickness at increasing Cl⁻ content were needed. For NaCN crystals thicknesses between 0.1 and 5 mm are necessary.

Due to the monotonous increase of the liquidus and solidus curves from the melting point of NaCN (837 K) to that of NaCl (1073 K) (Ref. 21) the CN⁻-to-Cl⁻ ratio within the crystal grown from the melt increases monotonically from the seed region to the opposite end. The difference between lowest and highest CN⁻ concentrations depends on the starting composition and the amounts of the melt and of crystallized material. Crystals were grown with lengths up to 10 cm and diameters of 1–2 cm.

Figure 2 represents a typical example for the strong variation of the CN⁻ concentration along the crystal length (crystal draw axis) as determined by the Debye-Scherrer method using the lattice constants as a probe for the concentration (see Fig. 1). The concentration is not symmetrically distributed around the ansatz of 70 mol% CN⁻ because a part of the material remained in the crucible and a part of the NaCN was lost by evaporation. All our measurements yield a concentration gradient of

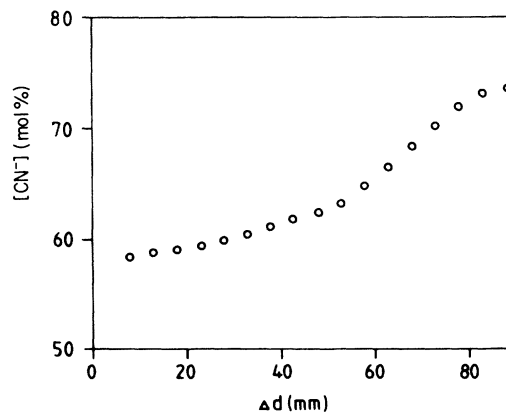


FIG. 2. Variation of the CN⁻ concentration along the draw axis of a Na(CN)_xCl_{1-x} single crystal. A melt ansatz of $x = 0.7$ was used. By Δd the distance from the edge (seed) of the sample is denoted.

about 0.3%/mm along the draw axis. Since samples with lateral dimensions of several millimeters are generally used in the ir spectrometer, the C-H-N analyzer and other classical methods such as neutron scattering and ultrasonic techniques, the correspondingly obtained experimental results always include an average over a significant concentration range. This is of particular importance for the interpretation of either the phase or the glass transitions.

The caloric behavior of $\text{Na}(\text{CN})_x\text{Cl}_{1-x}$ crystals was studied by differential scanning calorimetry (DSC) yielding most of the data given in the phase diagram (Fig. 3). In order to resolve the transition behavior in more detail, an automatized high-resolution adiabatic vacuum calorimeter²² was used to investigate samples with a size of about 1 cm^3 for concentrations $x = 1$, $x \approx 0.84$, and $x \approx 0.70$.

Besides a concentration gradient along the grow axis, a radial gradient of the CN^- concentration is also expected, with the highest CN^- concentration at the center line of the crystal. This is because the crystal adopts at the growth interface—due to the phase diagram—less CN^- than corresponds to the mean concentration in the melt. At the center of the interface the CN^- increase may be the highest due to the small convection speed resulting at this point from the rotation of the crystal. This expectation was confirmed by space-resolving Brillouin spectroscopy as will be shown in Sec. III.

Parts of the phase diagram of $\text{Na}(\text{CN})_x\text{Cl}_{1-x}$ were reported previously.^{5(a),13} The analysis of the caloric behavior (inset in Fig. 4) and light scattering experiments show that a crystal with $x = 0.65$ still undergoes a phase transition into a rhombohedral phase. These measurements were done on small parts of a large crystal previously used for NMR (Ref. 23) and neutron scattering experiments²⁴ which, in agreement with the behavior of c_{44} presented in Fig. 5 and discussed in Sec. III did not show any discontinuous phase transition. The disappearance of the first-order character of the phase transition near $x_c \approx 0.65$ is supported by the vanishing transition entropy (Fig. 4).

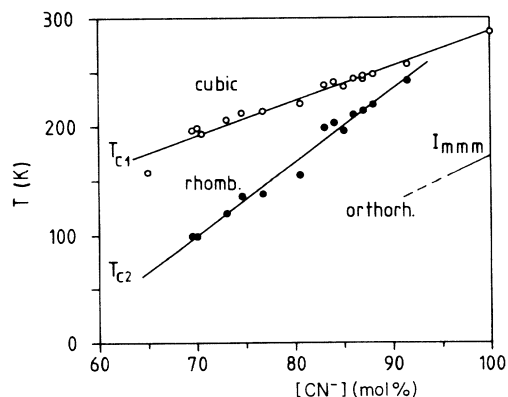


FIG. 3. Phase diagram of $\text{Na}(\text{CN})_x\text{Cl}_{1-x}$. The values of the phase-transition temperatures T_{c1} and T_{c2} were taken from DSC and dielectric measurements. The point at $x = 0.65$ is derived from the measurement shown in Fig. 4.

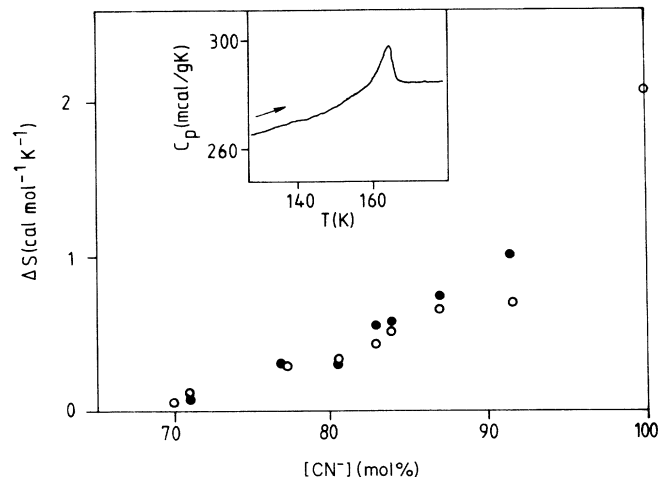


FIG. 4. Concentration dependence of transition entropies (open circle) at the cubic-orthorhombic ($x = 1$), the cubic-rhombohedral (dots), and the rhombohedral-orthorhombic (circles) phase transitions in $\text{Na}(\text{CN})_x\text{Cl}_{1-x}$ crystals. Inset shows DSC record for $x = 0.65$.

Some mixed crystal plates were investigated by Langtopography revealing a mosaic structure with grain sizes up to several mm. A point beam was scanned point by point across a grain boundary between two large grains measuring according to the bond method the (200) and (-200) reflexes. It followed that the two grains had almost the same lattice constant, and that the mosaic struc-

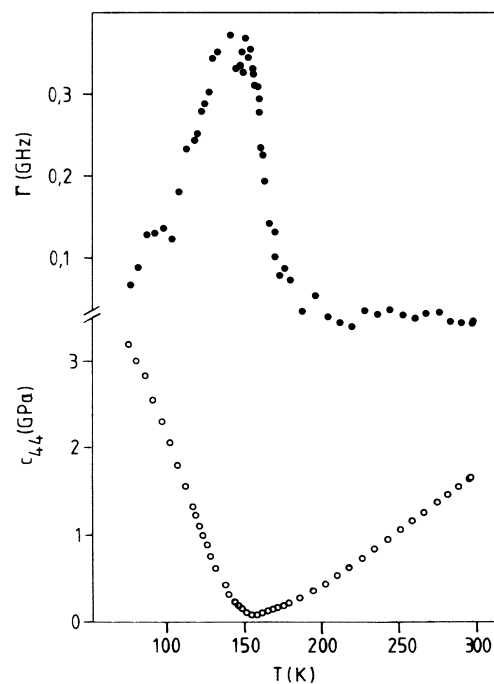


FIG. 5. Temperature dependences of the shear modulus c_{44} (circles) and hypersonic attenuation Γ (dots) for a sample with $x = 0.65 \approx x_c$. The minimum value of c_{44} is about 0.04 GPa. Note, that the $\Gamma(T)$ maximum occurs about 10 K below the minimum of $c_{44}(T)$; the latter coincides with the phase-transition temperature.

ture resulted from inclinations of the order of 0.5° between the two large grains. Within the grains the reflexes were rather sharp (0.08° with Mo $K\alpha$). Between the two large grains smaller ones were detected with dimensions below 1 mm and orientations monotonically changing between those of the large grains. Different crystals as well as different parts of the same crystal show different cleavage properties. Bad cleavage properties may be due to a distribution of the cubic axes of the grains.

For the interpretation of the elastic stiffness data we used an orthogonal reference frame with the x_1, x_2, x_3 axes parallel to the cubic directions of the samples. The stiffness coefficients c_{ij} (Voigt notation) of the mixed crystals were calculated using the densities obtained from the cell constants, measured with x-ray techniques and assuming rock salt structure at room temperature and supposing homogeneous CN^- distribution in a unit cell. The density was taken to be constant through the whole temperature range.

The Brillouin measurements were made with a high-performance Brillouin spectrometer using an argon-ion laser at the vacuum wave length $\lambda_0 = 514.5$ nm. The characteristics of this spectrometer were discussed elsewhere.²⁵ Figure 6 shows schematically the spectrometer setup that was used to obtain different realizations of the 90A- and 90R-scattering geometries^{17,26–29} described below. Using the shutters (SH indicated in Fig. 6) we could discriminate between these two types of scattering geometries. The platelike sample (SA in Fig. 6) could be rotated in a defined way around x_2 . The optical polarization conditions could be chosen using a Faraday rotator (FR) and a polarizer (PO).

The principles of the 90A- and 90R-scattering geometries have been discussed previously (e.g., Ref. 29). The main features of the scattering geometries are shown in Figs. 7(a) and 7(b), respectively. Using the 90A-method sound velocity polar plots can easily be obtained for sound wave propagation in the (x_1, x_3) plane of the sample by simply rotating it around x_2 (angular-resolving Brillouin technique). As long as the crystals under study

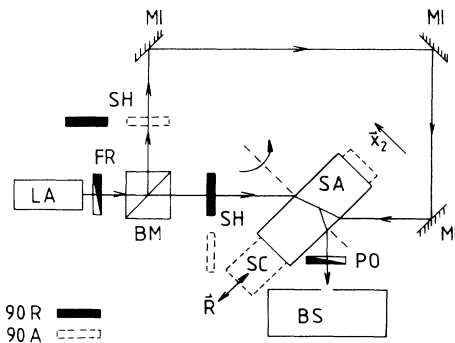


FIG. 6. Brillouin setup for a simultaneous measurement of different phonon modes. LA: argon ion laser; BM: beam splitter; FR: Faraday rotator; SH: shutters; SA: sample; MI: mirrors; PO: polarizer; BS: Brillouin spectrometer; SC: driven scan stage for space-resolving Brillouin spectroscopy; \mathbf{R} : driving direction; and \mathbf{x}_2 : unit vector along the x_2 axis of the sample coordinate system. The 90A and 90R methods are explained in the text and in Fig. 7.

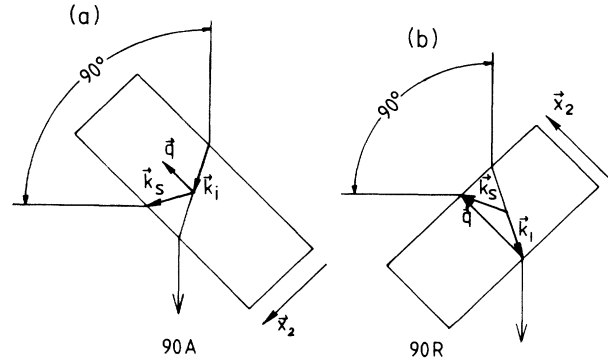


FIG. 7. Characteristics of the 90A- and 90R-scattering geometries [(a) and (b), respectively]. Outer scattering angle is 90° ; \mathbf{k}_i : wave vector of the incident laser beam; \mathbf{k}_s : wave vector of the scattered light; \mathbf{q} : phonon wave vector and \mathbf{x}_2 : unit vector along the x_2 axis of the sample coordinate system.

are of cubic symmetry the involved acoustic wave length for any direction of the sound wave vector \mathbf{q} is

$$\Lambda^{90A} = \lambda_0 / \sqrt{2}, \quad (1)$$

and does not depend on the optical properties of the sample. In contrast to the conventionally used scattering geometries, the sound velocity $v = f\Lambda$ depends only on the sound frequency f . Since the acoustic wavelength Λ does not depend on the refractive index of the cubic crystal, the 90A-scattering technique is the most appropriate to determine the elastic stiffness tensor. As a consequence, the related temperature-dependent elastic stiffness coefficient is given by $c(T) = \Lambda^2 \rho(T) f^2(T)$, where ρ is the mass density of the sample, and, in contrast to conventional Brillouin techniques, Λ is independent of temperature T . The typical reproducibility for the determination of the shear phonon frequency is about 0.2%.

For the 90R-scattering geometry, which is depicted in Fig. 7(b) for the case of a wave propagation along the x_2 axis, the relevant acoustic wavelength is

$$\Lambda^{90R} = \lambda_0 (4n^2 - 2)^{-1/2}, \quad (2)$$

where n is the refractive index of the sample. Using the experimental set up of Fig. 6 the 90A- and 90R-scattering geometries can be realized without changing the position and orientation of the crystal with respect to the apparatus simply by switching the shutters. In both cases the scattered light stems from nearly the same parts of the crystal. According to Fig. 7 for cubic crystals 90A- and 90R-scattering geometries select equivalent symmetry directions.

The 90A-scattering geometry allows us to use relatively thin samples.²⁹ Taking advantage of this fact, the scattering volume often can be located within only one domain of a polydomain sample yielding data of the single crystal. We have used this technique to measure elastic properties of $\text{Na}(\text{CN})_x\text{Cl}_{1-x}$ for $x = 1, 0.87, 0.73, 0.65$ for the noncubic phases. Furthermore, the spatial variation of the shear sound velocity measured by the 90A-scattering technique (spatial-resolving Brillouin spectroscopy) can be related to the in-

homogeneous structure of the sample.

Using a motor-driven scan stage (SC in Fig. 6) the scattering volume could be displaced through the sample along \mathbf{R} . The displacement could be measured with a precision of about $3 \mu\text{m}$; the scattering volume is roughly 10^{-7} cm^3 . This technique has been used to determine spatial concentration profiles in $\text{Na(CN)}_x\text{Cl}_{1-x}$.

Often the backscattering technique was used to investigate the elastic properties of mixed cyanide crystals.^{2,6} This method, besides having the advantage of a large scattering cross section and a small sensitivity to errors of scattering angles, has the following serious disadvantages: (i) unfavorable selection rules for the shear wave signal, (ii) the method generally probes within the scattering volume differently oriented domains in polydomain samples, and (iii) contrary to the $90A$ -scattering technique the acoustic wave vector involved depends on the refractive index and therefore implicitly on the temperature of the sample.

Provided the $90A$ - and the $90R$ -scattering geometries have been applied for symmetry equivalent directions of the cubic crystal, these geometries can be used to determine the opto-acoustic D^{90R} function.^{17,26,27} The D^{90R} function is a sensitive measure for the presence of hypersonic dispersion or in the absence of dispersion, yields directly the refractive index:^{17,27}

$$D_i^{90R}(\mathbf{x}_{\hat{q}}) = (\{ [f_i^{90R}(\mathbf{x}_2)/f^{90A}(\mathbf{x}_1)]^2 + 1 \} / 2)^{1/2}, \quad i = 1, 3. \quad (3)$$

$\mathbf{x}_{\hat{q}}$ represents directions of the cubic axes x_i ($i = 1, 2$) (it is understood that the acoustic wave vectors \mathbf{q} are directed along the cubic axes x_1 and x_2). As mentioned above, we can measure the sound frequencies $f_i^{90R}(\mathbf{q} \parallel \mathbf{x}_2)$ and $f^{90A}(\mathbf{q} \parallel \mathbf{x}_1)$ simultaneously from the same scattering volume (Fig. 6). If hypersonic dispersion can be neglected, this experimental procedure yields besides the stiffness moduli c_{11} and c_{44} , the refractive index n . The quantity $D_i^{90R} - n_i$ is a particular sensitive measure for hypersonic dispersion. For normal dispersion, $D_i^{90R} - n_i \geq 0$, holds. This probe for acoustic dispersion effects is of special interest if the phonon line widths are difficult to obtain or to interpret. This applies to the present case, particularly around and below the phase transition temperatures, where strong optical heterogeneities appear in the samples producing an additional broadening of the spectral lines. By means of the D^{90R} function one therefore derives information on hypersonic dynamics from the real part of the elastic stiffness.

In order to realize the opportunity to perform Brillouin measurements below the cubic phase thin samples were needed to overcome the optical problems (optical multiple scattering) with the polydomain structure (Sec. III). For this purpose cleaved crystal plates were carefully polished down to a thickness of about $200 \mu\text{m}$.

III. RESULTS AND DISCUSSION

A. Pure NaCN

The $90A$ -scattering method was used to determine the temperature dependence of the sound velocity of the transverse hypersonic mode around the cubic-

orthorhombic phase transition of NaCN. As mentioned in Sec. II, the $90A$ -scattering geometry yields for the cubic phase the correct hypersonic velocities independently of the refractive index of the sample. Figure 8 shows the resulting c_{44} data above $T_c = 284 \text{ K}$. In this case, for each temperature the values of the density given in the literature¹ were used to calculate the shear stiffness from the sound velocity data. The c_{44} data agree excellently with the Brillouin data of Wang and Satija³⁰ and Boissier *et al.*¹⁵ but deviate by about $+8\%$ from the ultrasonic data of Haussühl *et al.*¹ The ultrasonic data of Love *et al.*¹⁶ neither fit the Brillouin data nor the ultrasonic data of Ref. 1. To ensure that the discrepancies between hypersonic and ultrasonic measurements are not due to the quality of the crystals grown in different laboratories, we used the pulse echo method at 5 MHz to measure c_{44} on the same crystal used for our Brillouin experiments (inset in Fig. 8). Our ultrasonic c_{44} data are in rather good agreement with those of Ref. 1 although our temperature derivative $-dc_{44}/dT$ is slightly smaller. The latter discrepancy may be due to increasing mechanical constraints caused at decreasing temperature by the different thermal expansions of NaCN and the transducer including the bond material. To our experience this is a general problem in measuring the ultrasonic behavior of plastic crystals and soft glasses giving rise to results that are to some extent ambiguous. The discrepancies between ultrasonic and hypersonic data of NaCN have been attributed either to experimental inaccuracies,¹⁴ to impurities and domain walls,¹⁵ or to dispersion effects.¹⁶ In addition, hypersonic and ultrasonic results may suffer from the existence of mosaic structures (Sec. II). In any case, our experiments show that the differences cannot be explained by experimental errors.

The mosaic structure gives rise to spatial distributions of the cubic axes. As a consequence the apparent averaged stiffness modulus, c_{44}^u measured by ultrasonics is ex-

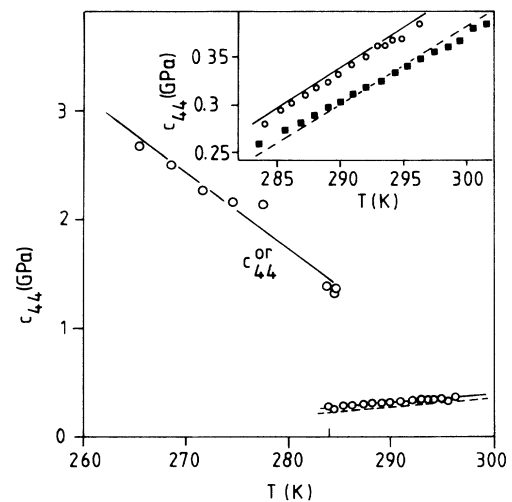


FIG. 8. Temperature dependence of the elastic moduli c_{44} and c_{44}^u above and below the ferroelastic phase transition of NaCN. The inset shows data obtained by different experimental techniques. Open circles: our Brillouin data. Solid line: Brillouin values of Ref. 23. Squares: our ultrasonic data. Dashed line: Ultrasonic data from Ref. 1.

pected to be larger than c_{44} of an ideal crystal. The stiffness modulus c_{44}^h measured by Brillouin spectroscopy is expected to be larger than c_{44} , too, if the phonon wave vector is tilted with respect to the cubic axis of the grain in the scattering volume. The (quantitative) effect of a spatial distribution of tilt angles on the experimental results, depends on the magnitude of the misorientation of the grains. Tilt angles up to 0.5° between the phonon wave vector and the cubic axis occurring in our samples (Sec. II), however, are too small to be resolved experimentally even by our high-performance Brillouin technique.

Generally the influence of hypersonic dynamics is investigated by inspecting the “phonon line width.” This method becomes insignificant if, as in our case, the attenuation is very small. We therefore determined the opto-acoustic D^{90R} function from the related sound frequencies (Sec. II). Figure 9 shows the corresponding squared sound frequencies and the D function. Since the D function depends linearly on the temperature and approximates well within the margin of error the refractive index function $n(T) = 1.4848 - 1.1068 \times 10^{-4}T$ (deduced from density data¹) there are no indications for hypersonic dynamics in our data even close to T_c . Therefore the reason for the discrepancies between c_{44}^u and c_{44}^h is not clear.

According to Fig. 10, the transition entropy appears in a temperature interval of about 0.5 K around T_c showing a two-peak structure. This indicates that the first-order transition is smeared out and that the sample under in-

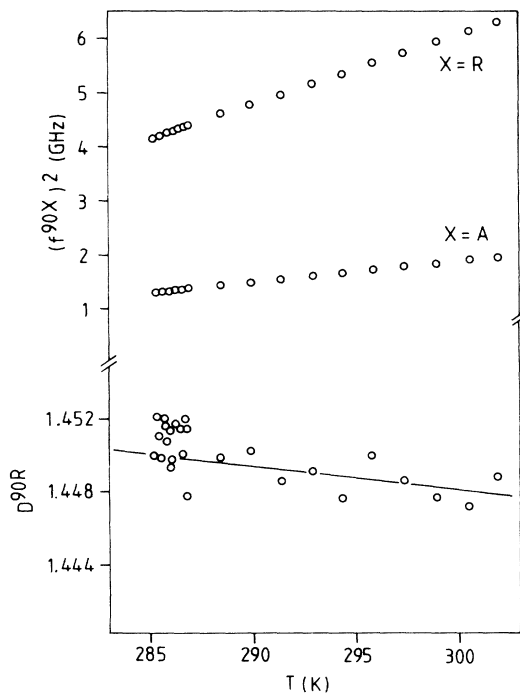


FIG. 9. Squared frequencies (top) for 90A- and 90R-scattering geometries and the opto-acoustic D^{90R} in NaCN above T_c . Within the experimental accuracy, the D function fits well to the refractive index data obtained from literature. A least-squares fit to our data yields the slope of $1.2 \times 10^{-4} \text{ K}^{-1}$.

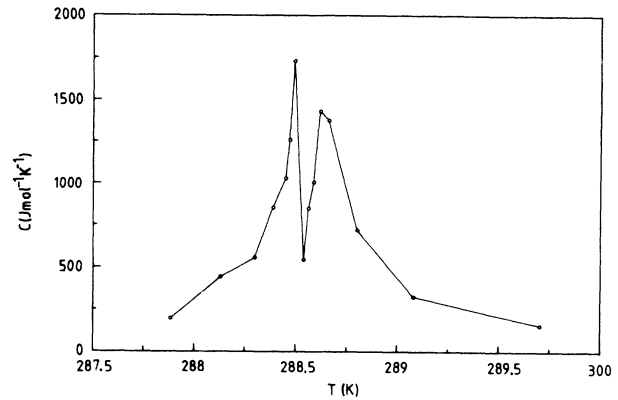


FIG. 10. Apparent molar heat capacity of a NaCN single crystal with a volume of about 10 mm^3 around T_c , measured in an adiabatic calorimeter at slow continuous heating.

vestigation is inhomogeneous. This behavior may possibly be related to internal stresses caused by the mosaic structure. The effects discussed here for pure NaCN are much less pronounced than the corresponding ones in the mixed cyanide crystals discussed below. Note that the distribution of T_c obtained for large samples in Fig. 10 is irrelevant for 90A- and 90R-Brillouin-scattering experiments that probe scattering volumes with a size of only 10^{-7} cm^3 and that are performed only on monodomain regions of the samples. The latter fact can always be checked by using the angular-resolving Brillouin technique (see Sec. II).

For the orthorhombic phase below T_c no c_{44} data exist for comparison. The elastic stiffness constant c_{44}^{or} given for that temperature range in Fig. 8 represents a quasishear mode. This results from the fact that although the corresponding spectra are obtained predominantly from one domain, we do not know exactly its orientation with respect to the scattering geometry. Furthermore, the mass density of the orthorhombic phase is not known. Therefore we have used the density at room temperature to calculate the c_{44}^{or} values. The smallness of c_{44}^{or} confirms the quasitransverse character of the measured mode.

Taking into account terms up to sixth order in the (scalar) order parameter the phenomenological Landau theory predicts for phase transitions of first order the following relations between the susceptibilities χ respectively their temperature derivatives both taken at T_c in the high- and low-temperatures phases:

$$\chi^{-1}|_{T=T_c-0} = 4\chi^{-1}|_{T=T_c+0}, \quad (4a)$$

$$\left. \frac{d\chi^{-1}}{dT} \right|_{T=T_c-0} = -8 \left. \frac{d\chi^{-1}}{dT} \right|_{T=T_c+0}. \quad (4b)$$

The corresponding experimental factors derived from Fig. 8 are about 5 and 8.2 and thus fit the predictions.

Several theoretical models have been introduced in order to describe the temperature and concentration dependence of the shear stiffness c_{44} . The theory of Michel^{18,19} takes into account the (collective) translation-rotation

coupling and random local strain fields. In other works^{8(a)} extensions of the theoretical results have been given and discussed. In the high-temperature region all these models result in the same temperature and concentration dependence, i.e.,

$$c_{44} = c_{44}^0 \frac{T - T_1 x [1 - x(1-x)T_3^2/T^2]}{T + T_2 x [1 - x(1-x)T_3^2/T^2]} \quad (5)$$

The parameters T_1, T_2, T_3 are related to those defined by Michel^{18,19} according to $T_1 = \delta y_w$, $T_2 = y_w(J + C^3)$, and $T_3^2 = \xi_w h^2$.

Clearly the background value c_{44}^0 does not reflect anharmonic properties. For pure NaCN ($x = 1$) Eq. (5) reduces to

$$c_{44} = c_{44}^0 \frac{T - T_1}{T + T_2} \quad (6)$$

According to Fig. 11 the c_{44} data can be fitted to a linear temperature dependence, i.e., a Curie-Weiss law with the Curie temperature 250.5 K and the Curie constant 1.181×10^{-7} K/Pa. The accuracy can be considerably improved if one fits according to Eq. (6). The resulting fit parameters are $c_{44}^0 = 14.9$ GPa, $T_1 = 253.4$ K, and $T_2 = 1436$ K. The value given by Boissier *et al.*¹⁵ for T_2 is about three times larger than ours. The large value of T_2 implies that in contrast to KCN (see Refs. 1, 2, and 31), in NaCN essentially a Curie-Weiss law holds. Since the deviations from the Curie-Weiss law are small from the statistical point of view, c_{44}^0 and T_2 in Eq. (6) are not completely independent. This means that changes in c_{44}^0 can partially be compensated by corresponding changes in T_2 .

The backscattering technique was used to determine the quasilongitudinal acoustic sound frequency f_{ql} of NaCN around the cubic-orthorhombic phase transition. For this measurement the acoustic wave vector q was

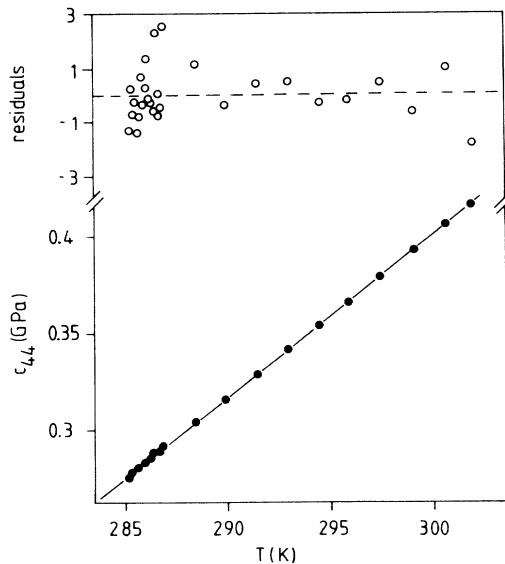


FIG. 11. Least-squares fit of Eq. (6) to the experimental data of pure NaCN (bottom). Corresponding residuals (top) are normalized by the standard deviation.

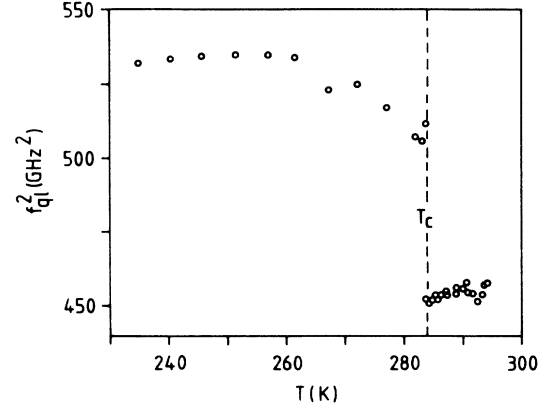


FIG. 12. Temperature dependence of the squared sound frequency f_{ql}^2 of a quasilongitudinal polarized phonon in NaCN. The values below the transition temperature $T_c = 284$ K. As discussed above, in the case of the shear mode, the temperature dependence of f_{ql}^2 below T_c gives only a qualitative picture because neither the number of different domains within the scattering volume nor their orientation with respect to the scattering geometry is known (disadvantage of the backscattering technique; see Sec. II). Nevertheless, comparing the sound frequency data of the low-temperature branch in Fig. 12 with those of the shear phonon below T_c , it seems clear that the low-temperature branch of f_{ql}^2 reflects a quasilongitudinal polarized phonon.

directed along (0.55,0.84,0) within the crystal. Figure 12 shows the resulting squared sound frequency data above and below the transition temperature $T_c = 284$ K. As discussed above, in the case of the shear mode, the temperature dependence of f_{ql}^2 below T_c gives only a qualitative picture because neither the number of different domains within the scattering volume nor their orientation with respect to the scattering geometry is known (disadvantage of the backscattering technique; see Sec. II). Nevertheless, comparing the sound frequency data of the low-temperature branch in Fig. 12 with those of the shear phonon below T_c , it seems clear that the low-temperature branch of f_{ql}^2 reflects a quasilongitudinal polarized phonon.

B. $\text{Na}(\text{CN})_x\text{Cl}_{1-x}$

As discussed in Sec. II the commonly used Czochralski growing procedure creates two major kinds of defects within the $\text{Na}(\text{CN})_x\text{Cl}_{1-x}$ crystals: (i) A significant concentration profile along the draw axis (Fig. 2)—the concentration profile perpendicular to the draw axis, however, was not known at the beginning of our investigations—and (ii) a mosaic structure with grains of diameters up to several millimeters—the cubic axis of adjacent large grains are inclined to each other. Both features may obscure the true elastic properties. We have therefore used the spatial- and angular-resolving Brillouin techniques discussed above to determine the distribution of these inhomogeneities in an orthogonal direction to the crystal grow axis.

90°-rotation measurements (Sec. II) were used to investigate the influence of sample inhomogeneities on the shear stiffness within sample regions slightly larger than the scattering volume. For this purpose the scattering volume was located a little bit away from the rotation axis of the sample holder. Rotating the sample, the scattering volume moves on a circle with a radius of about 150 μm . Figure 13 shows a typical sound velocity

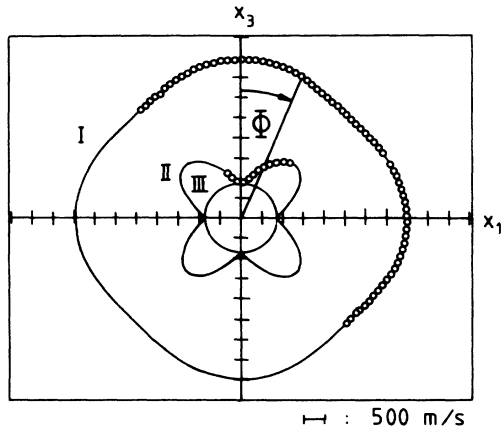


FIG. 13. Sound velocity polar plot measured at room temperature (295 K) for $\text{Na}(\text{CN})_{0.73}\text{Cl}_{0.27}$ for the phonon wave vector \mathbf{q} oriented in the (x_1, x_3) plane. $\Phi = \angle(\mathbf{q}, \mathbf{x}_3)$. I: Sound velocities of quasilongitudinal sound waves. II: Sound velocities of quasitransverse sound waves. III: Pure shear mode.

polar plot containing the measured data and a least-squares fit applied to the Christoffel equation (e.g., Refs. 32 and 33) assuming cubic symmetry. The resulting fit values are $c_{11} = (27.51 \pm 0.03)$ GPa, $c_{12} = (15.51 \pm 0.02)$ GPa, and $c_{44} = (1.303 \pm 0.009)$ GPa. Within the margin of error, the measured sound velocities vary completely continuously as a function of the rotation angle Φ . No breaks have been observed in the sound velocity polar plots measured on different samples until now. This indicates that on rotating the sample no different grains were involved having tilt angles greater than 0.5° between each other. Therefore our Brillouin data can be attributed to quasimonodomain regions.

Information about sample heterogeneities on a larger length scale can be obtained with space-resolving Brillouin techniques (Sec. II). This technique was used to measure the elastic shear stiffness perpendicular to the crystal draw axis. For this purpose we have used cleaved and polished platelike samples of about 1.5 mm thickness. To protect the sample surfaces against moisture and to diminish residual surface roughness the samples were located between glass slides with an immersion liquid between the sample surfaces and the glass slides. Then, surface domains as discussed by Gash *et al.*^{34,35} are expected not to be observed. Figure 14 shows the typical dependence of the sound velocity of the transverse-acoustic mode on the position of the scattering volume measured along a direction perpendicular to the draw axis.

One possible explanation relates the strong velocity gradient observed in Fig. 14 to a considerable concentration gradient. Figure 17, to be presented below, demonstrates that at room temperature c_{44} is a unique function of the concentration x . Therefore each sound velocity v_i in Fig. 14 can be related to a value x , thus establishing the relation between the concentration x and the position of the scattering volume within the crystal. The concentration shift Δx between the center and the boundary of the crystal plate would amount to about 3.5%. This cor-

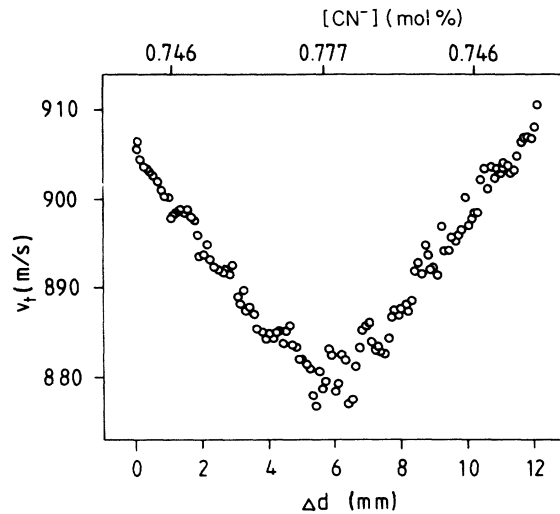


FIG. 14. Variation of the sound velocity of the transverse-acoustic mode measured at room temperature along a direction perpendicular to the draw axis. The relation between the shift parameter for the scattering volume Δd and the concentration x is explained in the text. Because of the relation between sound velocity and CN^- concentration, we can attribute the decreasing sound velocity to an increase in CN^- concentration. The lowest value for the sound velocity is placed in the center of rotation, where the seed was placed. The mean value in concentration for this sample lies around $x = 0.75$, with a change of $\Delta x = 0.035$ from the top to the bottom of the figure.

responds to a concentration gradient of about 0.7%/mm, which is of the same order of magnitude as was discussed above (Sec. II) for the concentration dependence along the draw axis (0.3%/mm).

By means of the phase diagram (Fig. 3) one ascribes the concentration profile of Fig. 14 to a distribution of phase transition temperatures T_c . The results of Fig. 14 then correspond to a T_c variation of about 10 K between the center and the boundary of the crystal plate. This T_c distribution has been confirmed by our high-performance calorimetric measurements: According to Fig. 15 the ap-

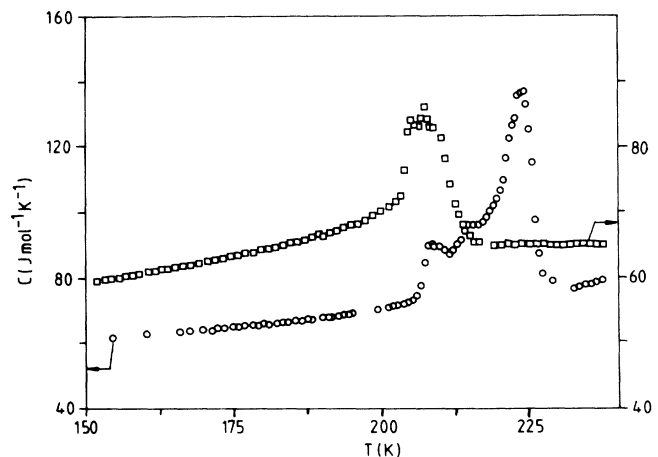


FIG. 15. Apparent molar heat capacity of $\text{Na}(\text{CN})_x\text{Cl}_{1-x}$ single crystals for $x = 0.7$ (squares) and $x = 0.84$ (circles) around the phase transitions.

parent molar heat capacity of $\text{Na}(\text{CN})_{0.7}\text{Cl}_{0.3}$ shows a latent heat distribution over about 10 K. Even larger T_c distributions of about 20 K have been observed for $\text{Na}(\text{CN})_{0.84}\text{Cl}_{0.16}$ (Fig. 15).

In addition, the peaks in the apparent molar heat capacity (Fig. 15) show some fine structure indicating the existence of domains with different transition temperatures. It is assumed that the concentration gradient within each domain is much smaller than the mean concentration gradient. Note that also in Fig. 14 some different levels of nearly constant concentration are apparent confirming the existence of such domains.

We conclude therefore the existence of pronounced concentration profiles in any direction of our Czochralski grown crystals. We believe that this is a general consequence of the growing technique and is not limited to crystals grown in our laboratory. In this context it would be of interest to know if other mixed crystals of the same family grown by the same technique behave differently from $\text{Na}(\text{CN})_x\text{Cl}_{1-x}$ crystals. Because of the small sized scattering volume used in our 90 A-Brillouin-scattering experiments, we are sure that our Brillouin data can be attributed to quasimonodomain regions. On the other hand, this statement generally does not hold if the physical informations are obtained from larger parts of the samples. This is the case, e.g., for caloric, ultrasonic, neutron-scattering, and NMR measurements.^{13,23,24}

We have measured the temperature dependence of the shear stiffness of $\text{Na}(\text{CN})_x\text{Cl}_{1-x}$ for the concentrations $x = 0.87, 0.73,$ and 0.65 by Brillouin spectroscopy (Fig. 16). Equation (5) has been applied to elastic data obtained for temperatures above the phase transition temperatures T_{c1} . For the general case of mixed crystals the theory contains, besides the variables concentration (x) and temperature (T), only parameters that are assumed to be the same for all concentrations. A reasonable way to determine these universal constants ($T_1, T_2, T_3,$ and c_{44}^0) is to use them as adjustable parameters in a least-squares fit applied simultaneously to all data sets corresponding to different concentrations. Because of the universality of $T_1, T_2,$ and c_{44}^0 , these values can be taken from the fit data of the pure system. Figure 16 shows the measured data for the above-mentioned different concen-

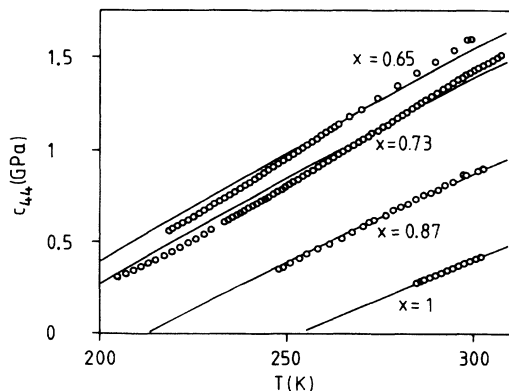


FIG. 16. Simultaneous least-squares fit for $x = 1, 0.87, 0.72,$ and 0.65 using Eq. (5). (Explanations are given in the text.)

trations and the corresponding simultaneously derived fit curves. The fit parameters obtained with this method are as follows: $T_3^2 = 221 \text{ K}^2$; for the concentrations $x = 0.87, 0.73, 0.65$ determined according to Fig. 1 the fit gives the corrected values $x = 0.84, 0.70, 0.67,$ respectively. Because of the space dependence of the concentration and the resulting uncertainty of this quantity within the scattering volume, we also allowed the concentrations to adjust themselves during the fit procedure, obtaining corrections on the assumed concentrations. As is seen from Fig. 16, the fit curves are in rather good agreement with the measured data in the case of high CN^- concentrations; the small deviations observed may be attributed to the neglect of the volume expansion and the inaccuracy in the absolute value of the density due to the uncertainty of the concentration used to calculate the shear elastic stiffness. The concentration corrections are very reasonable in accordance with the accuracy of our assumed concentrations. For lower CN^- concentrations the theory shows systematic deviations from the experimental values.

From Eq. (5) a critical concentration,

$$x_c^* = \frac{T_3^2}{T_3^2 + \frac{4}{27} T_1^2} \approx 2\% \quad (7)$$

defined by the conditions $c_{44} = 0$ and $dc_{44}/dT = 0$ [Refs. 8(a), 18, and 19] can be calculated. This value is far below the experimental value x_c . This result is to be expected because the inverse shear stiffness, although becoming extremely small (Fig. 5), does not diverge at T_c .

The question arises whether the systematic deviations between theory and experiment are due to the imperfections of the crystals or whether they are due to an inadequacy of Eq. (5) for low CN^- concentrations. The fact that similar problems have been reported by other authors for other cyanide mixed crystals^{6,7,8(b),36} may be taken as a hint that the crystal quality may not be the only reason for the observed discrepancies. To get a better agreement between the theory and the experimental data we introduced in a first step simple linear temperature and concentration dependences for the universal constants of the model. This approach, however, provided no improvements. In a second step we tried to improve the fit by adding a term linear in temperature $A(T - T_0)$ to Eq. (5), with A and T_0 depending on concentration. Following the same procedure as described above, we fitted the parameters ($T_3, x, A(x), T_0(x)$) fixing the remaining model parameters to those obtained for pure NaCN. As seen from Fig. 17 the fit is in excellent agreement with the experimental data. The fit values are given in Table I. Of course, the modification of Eq. (5) is empirical and is neither supported by Michel's theory nor can be confirmed by an obvious extension of this theory.

In case of $x = 0.87$ and 0.65 we succeeded in measuring the apparent shear stiffness below T_{c1} using thin crystal plates with a thickness of about $200 \mu\text{m}$. Figures 5 and 18 show the corresponding data. The transitions seen in these figures were, in addition, confirmed during the Brillouin investigations by a sudden appearance of optically efficient domains resulting in opaque samples. The

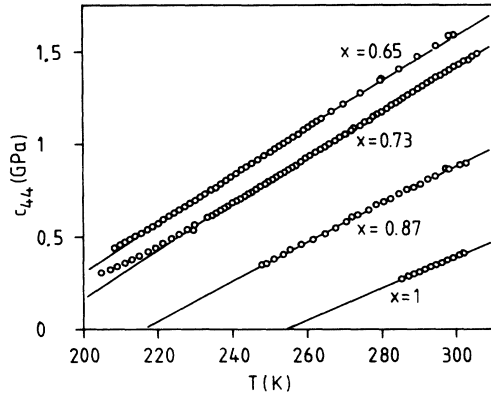


FIG. 17. Same as Fig. 16, improved by the addition of linear terms of the form $A(T - T_0)$. (For further explanations see text.)

opaqueness of thin samples, however, is tolerable because the sample plates consist of optically nearly homogeneous regions with lateral dimensions of about $150 \mu\text{m}$. Thus, the incident laser beam can relatively easily cross the sample using the 90° technique and allowing thus for Brillouin measurements on monodomain regions.

Since the densities of these samples are approximately known only at room temperature, we used these values to compute the c_{44} data for the whole temperature range. For the sample with $x = 0.87$, Brillouin experiments could be done for the cubic, the rhombohedral, and the orthorhombic phases. The transition temperatures determined with this method agree well with those measured using DSC (Fig. 3). The discontinuous elastic behavior confirms the first-order character of the phase transition. In addition, the c_{44} modulus tends to saturate with decreasing temperature below both transitions. For the same reasons as discussed in the case of pure NaCN, the c_{44} values below both transition temperatures can be interpreted only on a semiquantitative level.

As expected from Fig. 4, the amplitudes of the elastic discontinuities occurring at the ferroelastic phase transitions decrease with decreasing CN^- concentration. From the temperature behavior of the shear stiffness c_{44} measured at a sample of $x = 0.65$ (Fig. 5), no elastic discontinuity was observed although a first-order phase transition is still present (Fig. 4). The $c_{44}(T)$ curve behaves almost as in the glassy state.⁵

Despite the reduced optical quality of the sample with $x = 0.65$ an attempt was made to measure the hypersonic attenuation in the transition region. Approaching the

TABLE I. Values of fit parameters used in modification of Eq. (5).

| Concentration | | A (MPa/K) | T_0 (K) | T_3^2 (K ²) |
|---------------|-----------|-------------|-----------|---------------------------|
| Assumed | Corrected | | | |
| 0.87 | 0.83 | 1.6 | 288 | 425 |
| 0.73 | 0.71 | 1.7 | 286.9 | |
| 0.65 | 0.67 | 0.69 | 323.4 | |

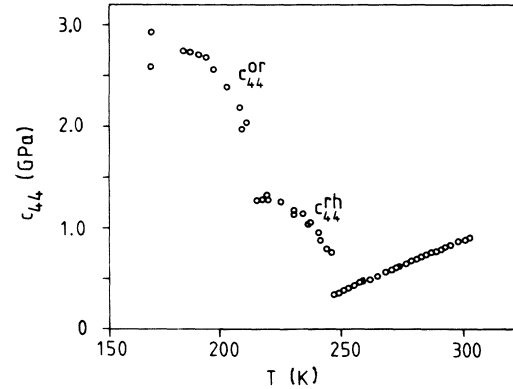


FIG. 18. Elastic stiffness coefficients c_{44} of $\text{Na}(\text{CN})_{0.87}\text{Cl}_{0.13}$ above and below the two transitions, cubic rhombohedral and rhombohedral orthorhombic. c_{44}^{rh} and c_{44}^{or} represent quasi-transverse polarized acoustic modes propagating within the low-temperature rhombohedral and orthorhombic phases, respectively.

phase transition T_{c1} from above, the phonon line width continuously increases. A certain part of this line broadening may be due to an increasing spread of the light beams within the sample due to interferences with domain boundaries at the border of the scattering volume. The hypersonic attenuation maximum appears about 10 K below T_{c1} at a frequency of about 1.15 GHz (Fig. 5). Taking into account that the sample reflects almost the glassy state it turns out that the dynamic glass transition temperature T_g^{dyn} ($= 147.5 \text{ K}$) is defined by the hypersonic loss maximum ($\omega\tau = 1$) rather than by the often used temperature of the $c_{44}(T)$ minimum.

IV. CONCLUSIONS

The elastic properties of $\text{Na}(\text{CN})_x\text{Cl}_{1-x}$ mixed crystals were investigated in the concentration range $1 \geq x \geq 0.65$ by high-performance Brillouin spectroscopy. Whereas the pure system NaCN shows a strong first-order ferroelastic phase transition, the critical concentration $x_c \lesssim 0.65$ characterizes the transition from a discontinuous phase transition to a continuous glass transition. The temperature and concentration dependences of the shear stiffness c_{44} reflecting the extremely elastic softening near the phase transition resembles those of other members of the same group of crystals with the composition $M(\text{CN})_x\text{Y}_{1-x}$. On the whole, a description of the elastic data of the high-temperature phase is possible by current theoretical models. With decreasing concentration x , however, increasing systematic deviations become apparent that might be caused at least partly by (i) spatial concentration variations on a mesoscopic scale, (ii) a re-normalization of the shear stiffness c_{44} due to relaxation processes at hypersonic frequencies, and (iii) a limited validity of the theoretical models for the class of materials under consideration.

As shown by space-resolving Brillouin studies of c_{44} , significant spatial concentration gradients exist in every direction of $\text{Na}(\text{CN})_x\text{Cl}_{1-x}$ samples, which are an una-

voidable consequence of the crystal growth technique applied and which principally cause a distribution of phase-transition temperatures in a macroscopic sample. Consequently the significance of results obtained on macroscopic samples is limited. This is corroborated by the reported calorific behavior. On the other hand, space-resolving Brillouin spectroscopy can be used to select sufficiently small scattering volumes that represent quasihomogeneous parts of the sample. It should be clarified by further investigations to which extent the physical properties of these quasihomogeneous parts are altered by their surroundings having different concentrations. The effect of hypersonic relaxation processes on the elastic shear stiffness as revealed by measurements of acoustic attenuation coefficients and opto-acoustic dispersion functions plays a significant role only for concentrations close to and below x_c . Hypersonic relaxation processes are therefore not the main sources for the deviations observed between the experimental data and the theoretical models.

The space-resolving Brillouin technique made it possi-

ble to measure the continuation of the shear mode below the orientational disordered cubic phase. The c_{44} discontinuities occurring at the ferroelastic transitions decrease with decreasing CN^- concentration and vanish close to the critical concentration x_c . In addition, the tendency of the shear stiffness $c_{44}(T)$ to saturate at lower temperatures disappears close to but above x_c . These results indicate that the physical properties of $\text{Na}(\text{CN})_x\text{Cl}_{1-x}$ mixed crystals still undergoing phase transitions already reflect properties of the glassy state appearing at $x \leq x_c$. Thus, detailed Brillouin investigations of these systems at concentrations for which the glass transition occurs are highly desirable.

ACKNOWLEDGMENTS

The authors would like to thank K. H. Michel, C. W. Garland, and R. Blinc for exciting and fruitful discussions. One of the authors (R. Jiménez) is indebted to the Spanish government for supporting his activities (beca F.P.I. PG 89 00802408).

- ¹S. Haussühl, J. Eckstein, K. Recker, and F. Wallrafen, *Acta Crystallogr. A* **33**, 847 (1977).
- ²W. Rehwald, J. R. Sandercock, and M. Rossinelli, *Phys. Status Solidi A* **42**, 699 (1977).
- ³S. K. Satija and C. H. Wang, *Solid State Commun.* **28**, 617 (1978).
- ⁴(a) K. Knorr, *Phys. Scr. T* **19**, 531 (1987); (b) U. G. Volkmann, R. Böhmer, A. Loidl, K. Knorr, U. T. Höchli, and S. Haussühl, *Phys. Rev. Lett.* **56**, 1716 (1986).
- ⁵(a) S. Elschner, J. Petersson, J. Albers, and J. K. Krüger, *Ferroelectrics* **78**, 43 (1988); (b) R. Jiménez, K.-P. Bohn, J. K. Krüger, and J. Petersson, *ibid.* **106**, 175 (1990).
- ⁶J. F. Berret, A. Farkadi, M. Boissier, and J. Pelous, *Phys. Rev. B* **39**, 13 451 (1989).
- ⁷Z. Hu, D. Walton, and J. J. Vanderwal, *Phys. Rev. B* **38**, 10 830 (1988).
- ⁸(a) J. O. Fossum, A. Wells, and C. W. Garland, *Phys. Rev. B* **38**, 412 (1988); (b) J. O. Fossum and C. W. Garland, *J. Chem. Phys.* **89**, 7441 (1988).
- ⁹G. D. Patterson, *Methods of Experimental Physics* (Academic, New York, 1980), Vol. 16A, pp. 170.
- ¹⁰J. K. Krüger, in *Optical Techniques to Characterize Polymer Systems*, edited by H. Bässler (Elsevier, Amsterdam, 1989).
- ¹¹J. Albers, Sonderforschungsbereich 130, University of Saarbrücken, report, 1985 (unpublished).
- ¹²S. Elschner, doctoral thesis, University of Saarbrücken, 1986.
- ¹³S. Elschner, K. Knorr, and A. Loidl, *Z. Phys. B* **61**, 209 (1985).
- ¹⁴S. K. Satija and C. H. Wang, *J. Chem. Phys.* **70**, 4437 (1979).
- ¹⁵M. Boissier, R. Vacher, D. Fontaine, and R. M. Pick, *J. Phys. (Paris)* **41**, 1437 (1980).
- ¹⁶W. F. Love, H. D. Hochheimer, M. W. Anderson, R. N. Work, and C. T. Walker, *Solid State Commun.* **23**, 365 (1977).
- ¹⁷J. K. Krüger, L. Peetz, R. Siems, H. G. Unruh, M. Eich, O. Hermann-Schönherr, and J. H. Wendorff, *Phys. Rev. A* **37**, 7 (1988).
- ¹⁸K. H. Michel, *Phys. Rev. B* **35**, 1405 (1987).
- ¹⁹K. H. Michel, *Phys. Rev. B* **35**, 1414 (1987).
- ²⁰G. Natta and L. Passerini, *Gazz. Chim. Ital.* **61**, 191 (1931).
- ²¹W. Truthe, *Z. Anorg. Chem.* **76**, 138 (1912).
- ²²E. Sauerland, J. Helwig, and H. E. Müser, *Thermochim. Acta* **69**, 253 (1983).
- ²³S. Elschner and J. Petersson, *Z. Naturforsch.* **41a**, 343 (1987).
- ²⁴S. Elschner, J. Albers, A. Loidl, and J. K. Krüger, *Europhys. Lett.* **4**, 1139 (1987).
- ²⁵J. K. Krüger, R. Kimmich, J. Sandercock, and H.-G. Unruh, *Polym. Bull.* **5**, 615 (1981).
- ²⁶J. K. Krüger, A. Marx, R. Roberts, H.-G. Unruh, M. B. Bitar, H. Nguyen-Trong, and H. Seliger, *Makromol. Chem.* **185**, 1469 (1984).
- ²⁷J. K. Krüger, A. Marx, L. Peetz, R. Roberts, and H.-G. Unruh, *Colloid Polym. Sci.* **264**, 403 (1986).
- ²⁸J. K. Krüger, L. Peetz, and M. Pietralla, *Polymer* **19**, 1397 (1978).
- ²⁹J. K. Krüger, L. Peetz, W. Wildner, and M. Pietralla, *Polymer* **21**, 620 (1980).
- ³⁰C. H. Wang and S. K. Satija, *J. Chem. Phys.* **67**, 851 (1977).
- ³¹M. Boissier, R. Vacher, D. Fontaine, and R. M. Pick, *J. Phys. (Paris)* **39**, 205 (1978).
- ³²J. K. Krüger, C. Grammes, and J. H. Wendorff, in *Dynamics of Disordered Materials*, Vol. 37 of *Springer Proceedings in Physics*, edited by D. Richter, A. J. Dianoux, W. Petry, and J. Teixeira (Springer-Verlag, Berlin, 1989).
- ³³B. A. Auld, *Acoustic Fields and Waves in Solids* (Wiley, New York, 1973).
- ³⁴P. W. Gash, *J. Appl. Phys.* **54**, 6900 (1983).
- ³⁵P. W. Gash and F. Lüty, *J. Microsc.* **140**, 351 (1985).
- ³⁶Z. Hu, C. W. Garland, and A. Wells, *Phys. Rev. B* **40**, 5757 (1989).